JOURNAL OF MATERIALS SCIENCE 28 (1993) 2517–2530

Spheroidal inclusion effects on acoustic emission–microstructural relations in ferritic steels

H. N. G. WADLEY*, C. B. SCRUBY
National NDT Centre, AEA Technology, Harwell Laboratory, Oxfordshire, UK

A comparison of the acoustic emission accompanying the deformation and fracture of high- and low-sulphur steels subjected to various heat treatments has revealed that an additional component of acoustic emission exists in steels with high manganese sulphide inclusion content. The inclusion component of the emission has been correlated with matrix properties and shows some dependence upon yield strength. Results are consistent with both interfacial decohesion and microplasticity in the ensuing region of matrix-stress intensification acting as the source of the extra acoustic emission signals. The results also shed light upon the ways in which inclusion and carbide distributions interact to influence the ambient-temperature fracture mode. In particular, there is a transition from an alternating shear to a cup and cone fracture mode as the carbide size increases. The quasi-static ductile-dimple mechanism of the cup and cone fractures does not generate detectable signals. The unstable alternating shear fracture is found to be capable of generating detectable signals, an observation that has important consequences for attempts to utilize acoustic emission for the detection of crack growth.

1. Introduction

When combined with systematic microstructural variation, acoustic emission monitoring during mechanical testing affords an interesting opportunity to gain new insights into deformation and fracture phenomena [1–3]. In two earlier papers [4, 5], we reported the application of this approach to the study of deformation and fracture mechanisms in ferritic steels. Model low-alloy steels of varying carbon content and uniformly low (0.0059%) sulphur content were subjected to a wide variety of quenching and tempering treatments to produce a broad spectrum of microstructures that were subsequently mechanically tested and their acoustic emission studied. The low sulphur content coupled with limited high-temperature deformation of the as-cast material resulted in a small volume fraction of approximately spheroidal MnS inclusions in these earlier materials. This enabled matrix slip and fracture mechanisms to be studied with minimal (but not totally eliminated) inclusion effects. It was found that lightly tempered microstructures emitted copious acoustic emission at yield. The results suggested that a process such as precipitate shear was activated when precipitates were very small (~ 10 nm).

In engineering steels, inclusions play a key role in ductile fracture processes [6, 7] although the mechanisms are still not precisely understood. Inclusions have also been proposed to be a source of detectable acoustic emission during otherwise silent ductile crack extension in engineering structures [8, 9]. The purpose of the work reported here was to gain a deeper insight into the role of the inclusions regarding acoustic emission during deformation and fracture. By repeating the tests reported earlier [5] with steels containing a ten-fold increase in sulphur concentration, we have the opportunity to separate the contribution of the inclusions from that of the matrix. The study reveals a small addition to the acoustic emission that is indeed related to inclusion–matrix decohesion. It also provides clear evidence of synergistic interactions between inclusions and matrix plasticity, which, during the period of non-uniform elongation prior to fracture, extends the range of carbide distributions that lead to unstable alternating shear fracture.

2. Experimental procedure

In order that the matrix microstructure and inclusion contributions to the results could be separated, a series of three model low-alloy steels were prepared with a similar composition (other than sulphur) to those studied earlier [4, 5]. Each steel was prepared by vacuum melting electrolytic iron with high-purity alloy additions, and casting into 150 kg ingots, 150 mm × 150 mm cross-section and 600 mm long. Chemical analyses for the three steels are given in Table I. Compared with Steels D, E and F of the

* *Present address*: Department of Materials Science and Engineering, University of Virginia, Charlottesville, VA 22903, USA.

TABLE I Chemical composition of high-sulphur steels

	Element (wt %)							
	C	S	N	O	Ni	Mn	Si	Cu
Steel A	0.054	0.069	0.003	0.003	3.26	1.03	0.53	0.02
Steel B	0.197	0.070	0.003	0.003	3.26	1.03	0.47	0.02
Steel C	0.494	0.069	0.003	0.003	3.26	1.03	0.46	0.02

P < 0.005, Cr, Mo, Al, Ti, V, Co, Zn, As, Zr, Nb, Sn, Bi < 0.01 wt %.

earlier study [4], these contained approximately an order of magnitude more sulphur. Apart from very small differences in carbon content they were otherwise identical to their low-sulphur counterparts.

A 150 mm length billet was cut from each ingot, heated to 1200 °C and then hot forged with a 3:1 reduction. Identical procedures to the earlier study were then used to machine cylindrical dumb-bell tensile samples from these bars. These samples were heat treated, again in the same manner as before for the low-sulphur steels [5] to give new sets of samples, i.e. they were first austenitized, then oil quenched, and one set subsequently isochronally tempered for 100 min between 50 and 600 °C, while the second was tempered isothermally at 625 °C for between 10 and 40,000 min.

Acoustic emission was measured during constant strain-rate mechanical testing. Great care was taken to ensure that quantitative comparisons could be made with earlier work. This involved maintenance of all instrumentation settings, calibration of each run with a standard source, and multiple tests to average some of the statistical fluctuation.

3. Results

3.1. Microstructural characterization

Optical microscopy and transmission electron microscopy indicated that the only significant difference between the steels of this study and the low-sulphur steels of the previous work [5] was the greatly increased density of inclusions. No significant differences in grain size, recrystallization or precipitation kinetics were observed.

The manganese sulphide inclusions were of two types, Fig. 1. The majority of inclusions were of the so-called Type II, Fig. 1a. These had formed at interdendritic interstices during the final stages of solidification. They were spheroidal or ellipsoidal with aspect ratios typically around 2:1, and formed a network covering the interconnected prior dendrite surfaces. The remaining inclusions were randomly distributed spheroids, Fig. 1b. They were typically smaller than those of the Type II distribution. Upon deformation, the Type II inclusions acted as primary nucleation sites for voids, Fig. 2. In all three steels, the inclusion size distribution was similar, Fig. 3, and the aspect ratio did not change.

At high temperatures (> 1100 °C) the malleability of the steel matrix exceeds that of the inclusions, so that little inclusion deformation occurs during hot work. The small, high-temperature forging reduction caused only a relatively small reorientation and elongation of the inclusions. These steels thus possessed a relatively equiaxed, spheroidal inclusion distribution, at least when compared with more typical commercial steels that undergo a larger but cooler hot rolling reduction in area.

3.2. Acoustic emission measurements

Representative stress–strain curves with acoustic emission superimposed are shown for isochronally tempered samples in Figs 4 and 5. It is found that, within sample to sample scatter, high- and low-sulphur steels exhibit almost identical dependence of

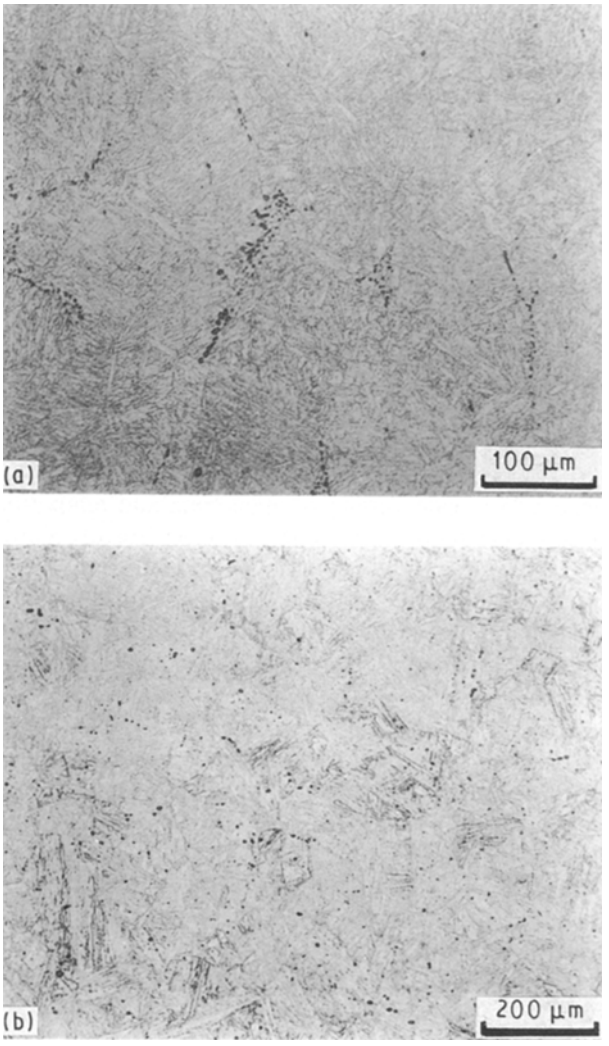

Figure 1 Micrographs showing distribution of manganese sulphide inclusions. (a) Type 2 interdendritic sulphides, (b) random distribution of spheroidal sulphides.

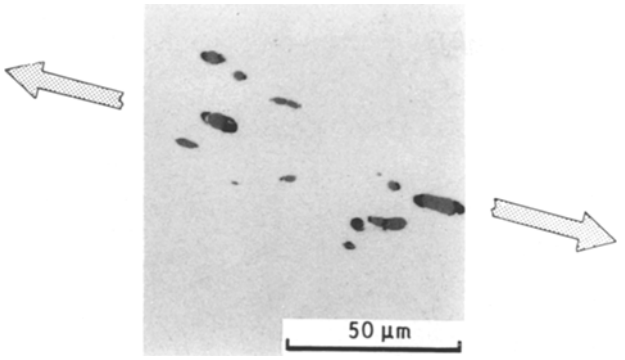

Figure 2 Decohesion at poles of inclusions after deformation.

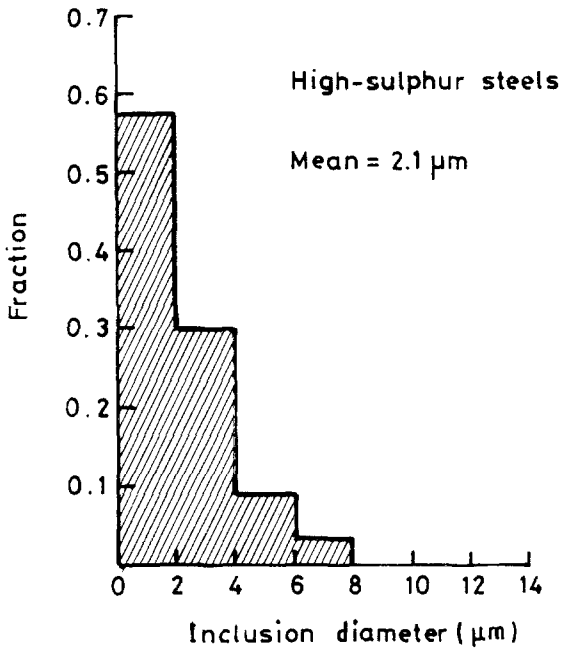

Figure 3 Inclusion size distribution for Steels A, B, C, obtained from analysis of 100 inclusions in each steel.

acoustic emission power upon strain and heat treatment. The only significant differences we have been able to systematically observe between high- and low-sulphur steels is a tendency for increased acoustic emission signal intensity just prior to fracture in medium- and high-carbon samples (e.g. Fig. 5c) and a slightly greater emission intensity in high-sulphur samples (see below). The data were very carefully examined to see if there was any evidence of inclusion-related emissions over strain ranges that were not masked by other emission-generating processes, but none was found.

For comparison purposes, the emission energy associated with plastic deformation (up to σ_{UTS}, Region I) and fracture (post σ_{UTS}, Region II) was determined for each test. The averages from four identical samples are given for each heat treatment in Table II. The data for Region I are plotted and compared with equivalent data for low-sulphur steels in Fig. 6. It can now be seen that high-sulphur steels consistently generate more emission energy than their low-sulphur counterparts. The exception appears to

TABLE II Plastic-deformation generated acoustic emission as a function of isochronal tempering

Region	Heat treatment (100 min)	Acoustic emission energy (mJ) Steel A	Steel B	Steel C
I	Oil quench	1.4	0.7	[a]
	Oil quench + 49 °C	1.5	0.5	[a]
	Oil quench + 97 °C	1.0	1.1	[a]
	Oil quench + 145 °C	2.0	6.8	4.0
	Oil quench + 197 °C	17.7	11.9	11.9
	Oil quench + 287 °C	34.1	40.0	39.0
	Oil quench + 403 °C	17.5	18.3	29.8
	Oil quench + 502 °C	2.7	5.8	13.3
	Oil quench + 601 °C	1.9	2.3	5.1
II	Oil quench	0.5	0.8	6.6
	Oil quench + 49 °C	0.5	0.6	11.2
	Oil quench + 97 °C	0.4	0.5	16.2
	Oil quench + 145 °C	0.5	0.5	30.0
	Oil quench + 197 °C	0.5	0.6	3.0
	Oil quench + 287 °C	0.5	0.6	1.7
	Oil quench + 403 °C	0.4	0.5	0.8
	Oil quench + 502 °C	0.4	0.5	1.0
	Oil quench + 601 °C	0.3	0.4	0.6

[a]Fracture before onset of plastic deformation (acoustic emission attributed to Region II).

TABLE III Plastic deformation generated acoustic emission (Region I) as a function of isothermal tempering

Heat treatment	Acoustic emission energy (mJ) Steel A	Steel B	Steel C
Oil quench	1.4	0.7	[a]
Oil quench + 625 °C, 5 min	9.6	30.4	18.23
Oil quench + 625 °C, 10 min	3.4	5.3	12.3
Oil quench + 625 °C, 40 min	2.0	3.2	5.46
Oil quench + 625 °C, 100 min	2.0	2.3	3.00
Oil quench + 625 °C, 400 min	1.8	2.6	2.95
Oil quench + 625 °C, 1000 min	0.9	0.5	3.47
Oil quench + 625 °C, 4000 min	0.4	0.5	3.70
Oil quench + 625 °C, 10000 min	0.9	1.7	4.45
Oil quench + 625 °C, 40000 min	0.7	1.2	1.92

[a]Elastic fracture, all emission (7.1 mJ) assigned to Region II.

be high-carbon material tempered below ~250 °C, where brittle fracture dominates.

The emission energy for isothermally tempered samples is given in Table III. High-sulphur samples of isothermally tempered steels once again usually generated significantly more acoustic emission energy than their low-sulphur counterparts, Fig. 7. The observations indicate that, in the vicinity of yield where most emission occurs, an additional source of acoustic emission exists in high-sulphur steels of medium- and high-carbon concentration.

3.3. Mechanical properties

Load and displacement values during constant strain rate tensile tests were digitally recorded for each heat treatment. These records were analysed to determine mechanical property parameters, which are given in

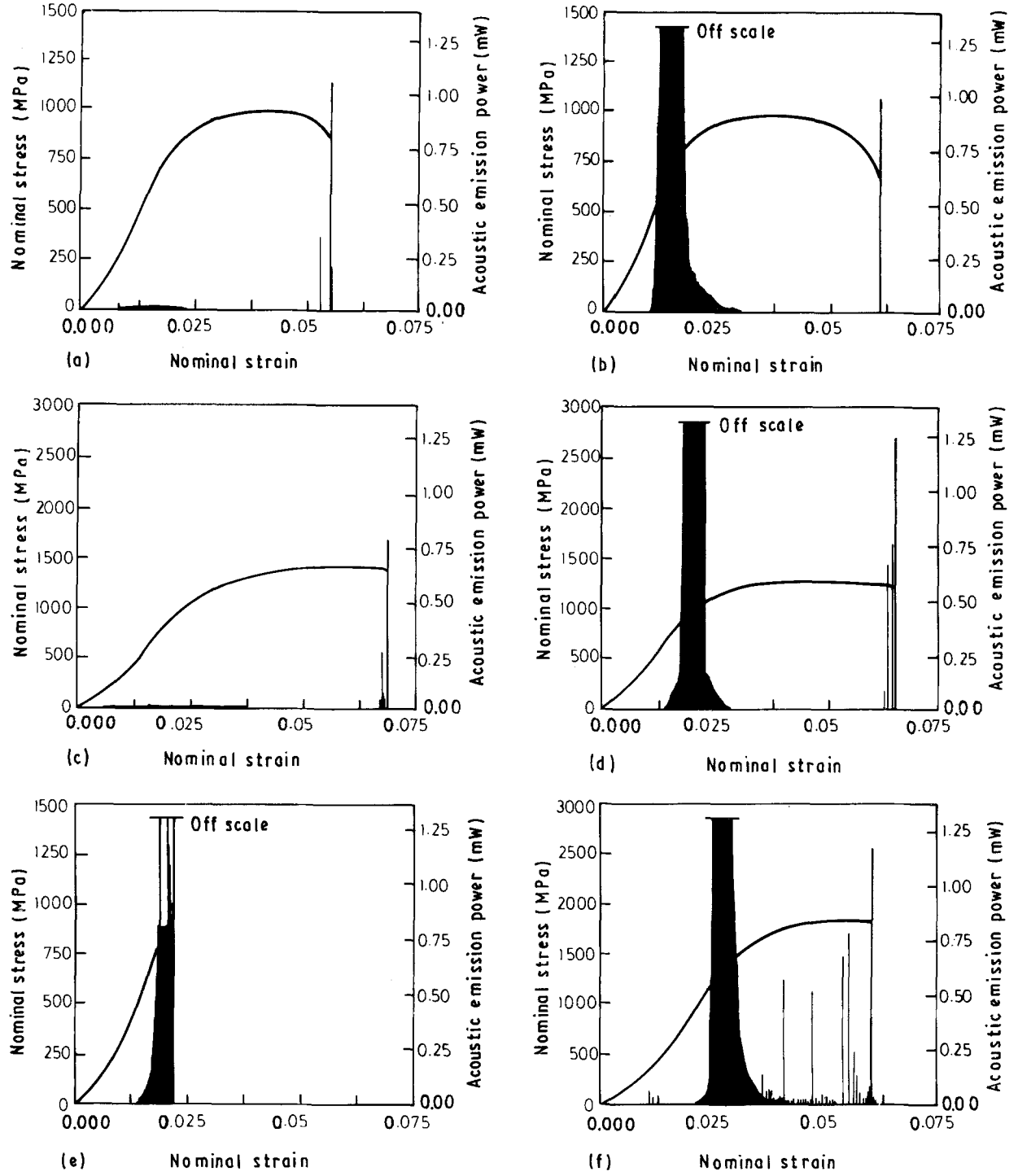

Figure 4 Typical stress–strain data with acoustic emission superimposed for high-sulphur steels isochronally tempered at (a, c, e) 97 and (b, d, f) 287 °C for 100 min. (a, b) 0.054% C, (c, d) 0.197% C, (e, f) 0.494% C.

Tables IV and V. Comparisons with equivalent low-sulphur steel data (Figs 8 and 9), indicate that the yield and ultimate tensile stresses are basically unaffected by an increase in sulphur content. The small discrepancies in strength between high- and low-sulphur material are smaller than the (small) strength differences due to carbon concentration variation between steel pairs. Both sets of steels were also found to have very similar work-hardening rates (and exponents) during initial deformation (values at 1% strain are tabulated). We have noted that the strain to attainment of maximum nominal stress (ε_{UTS}) is usually less for the high-sulphur steels, but the trends with heat treatment remained similar to low-sulphur steel.

The most significant difference between high- and low-sulphur steels is a significantly reduced non-uniform (or post σ_{UTS}) strain in the high-sulphur steels. For example, the average post σ_{UTS} extensions to fracture for the isochronally tempered steel series is 0.83 and 1.43 mm for Steels A and D, respectively. This post-σ_{UTS} deformation is also a strong function of heat treatment exhibiting a minimum for tempering temperatures $\sim$200 °C. The non-uniform extension also decreased with increasing carbon content. These observations point to a role for both the volume fraction of inclusions and the matrix plasticity in determining the extent of non-uniform deformation in this class of steels.

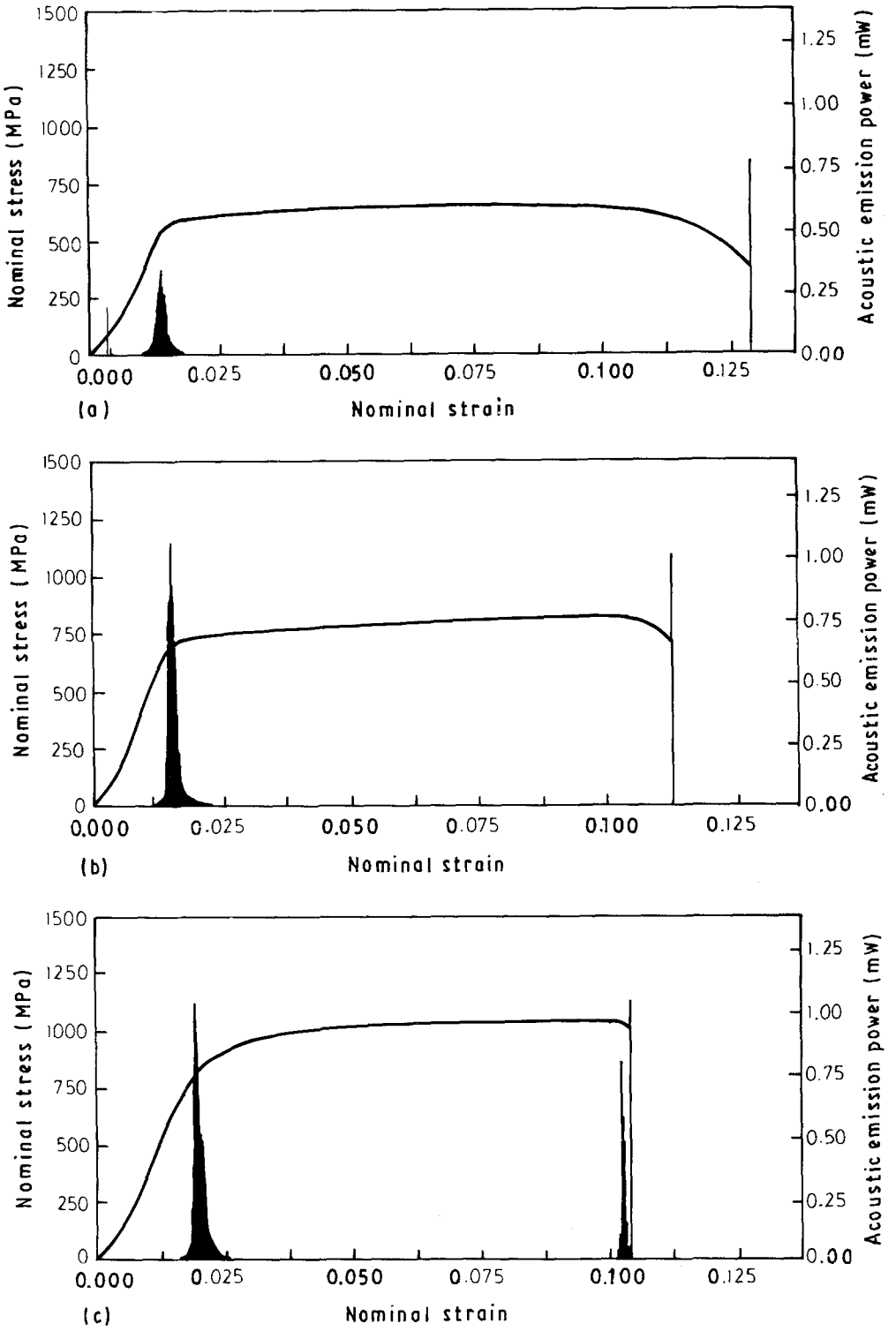

Figure 5 Typical stress–strain and acoustic emission data for isochronal tempering at 502 °C. (a) 0.054% C, (b) 0.197% C, (c) 0.494% C.

3.4. Fractography

The macroscopic fracture mode varied considerably with carbon content and tempering treatment (Figs 10 and 11). The overall trend for high-sulphur steels is summarized in Table VI.

3.4.1. Cup and cone fracture

Those samples that fractured by the cup and cone process usually contained a bimodal void-size distribution (Fig. 12). One component consisted of large, centrally located voids (tens of micrometres in diameter) that were associated with manganese sulphide inclusions. The diameter and depth of these voids usually increased with the size of the inclusion. The second component consisted of small voids (a few micrometres in diameter), uniformly distributed over the inter-inclusion ligaments. The density of the voids belonging to this component of the void population was closely related to the volume fraction of optically resolvable (i.e. > 0.5 μm) carbides.

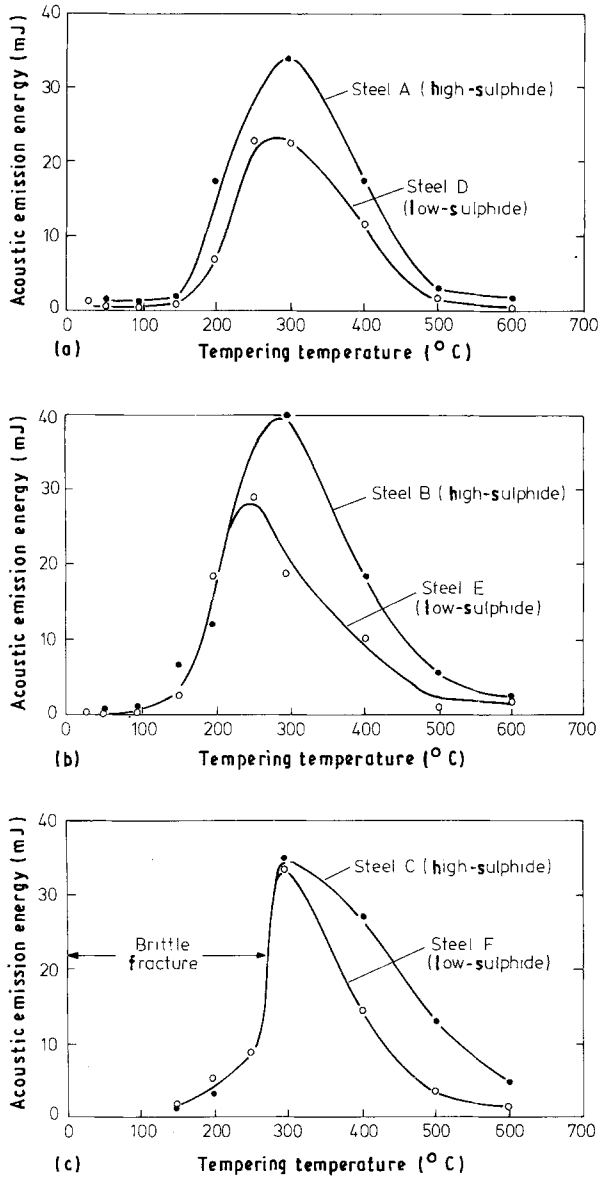

Figure 6 Dependence of Region I acoustic emission upon tempering temperature and carbon concentration for low- and high-sulphur steels. (a) Low-carbon, (b) medium-carbon, (c) high-carbon content.

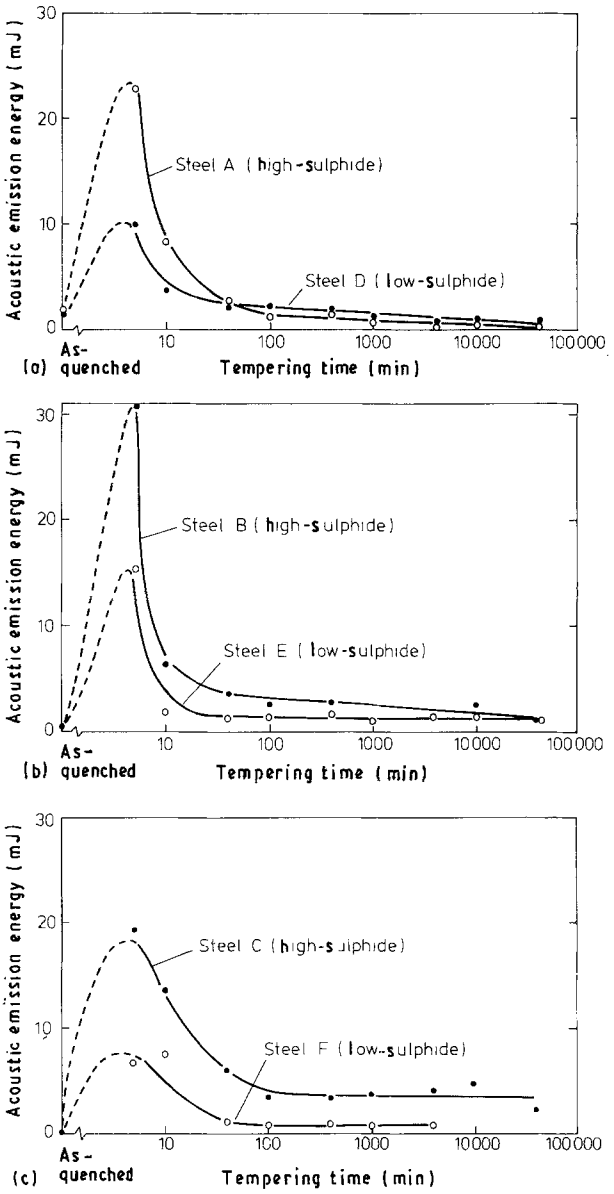

Figure 7 Dependence of acoustic emission upon isothermal tempering at 625 °C and carbon concentration for low- and high-sulphur steels. (a) Low-carbon, (b) medium-carbon, (c) high-carbon content.

One explanation for such observations is that voids are easily nucleated at the weak interfaces of larger inclusions, and grow steadily during subsequent plastic flow. In material containing few large carbides, the inter-inclusion ligaments internally neck smoothly without further void formation other than at smaller spheroidal sulphides. However, when larger carbides are present, those within the inter-inclusion ligaments act as sites for further microvoid nucleation. If the void radius is indicative of post-nucleation strain these carbide-nucleated voids appear to have nucleated considerably later than those at inclusions.

3.4.2. Alternating shear fracture

Voids of moderate depth (but less than those of the cup and cone fractures) were observed to have nucleated primarily at manganese sulphide inclusions, in samples that fracture by the alternating shear mechanism (Fig. 13). However, instead of the inter-inclusion ligaments undergoing extensive necking, unstable shear occurred between groups of longitudinally displaced voids. This process results eventually in the formation of a shear plane on the fracture surface. The next shear interlinkage usually occurs in the alternate direction in such a way that inclined shear facets cover the fracture surface, the average fracture path remaining approximately normal to the loading direction.

It is clear that this mode of fracture is also linked to the underlying spatial distribution of inclusions and to the metallurgical state of the interinclusion matrix. For example, by increasing the tempering temperature of steels B and C, it was possible to induce a transition from alternating shear to cup and cone fracture. The required tempering temperature, however, depended on sulphide concentration. Whilst Steel B underwent this transition at ~500 °C (low-sulphur), Steel E underwent cup and cone fracture after tempering at temperatures as low as 250 °C.

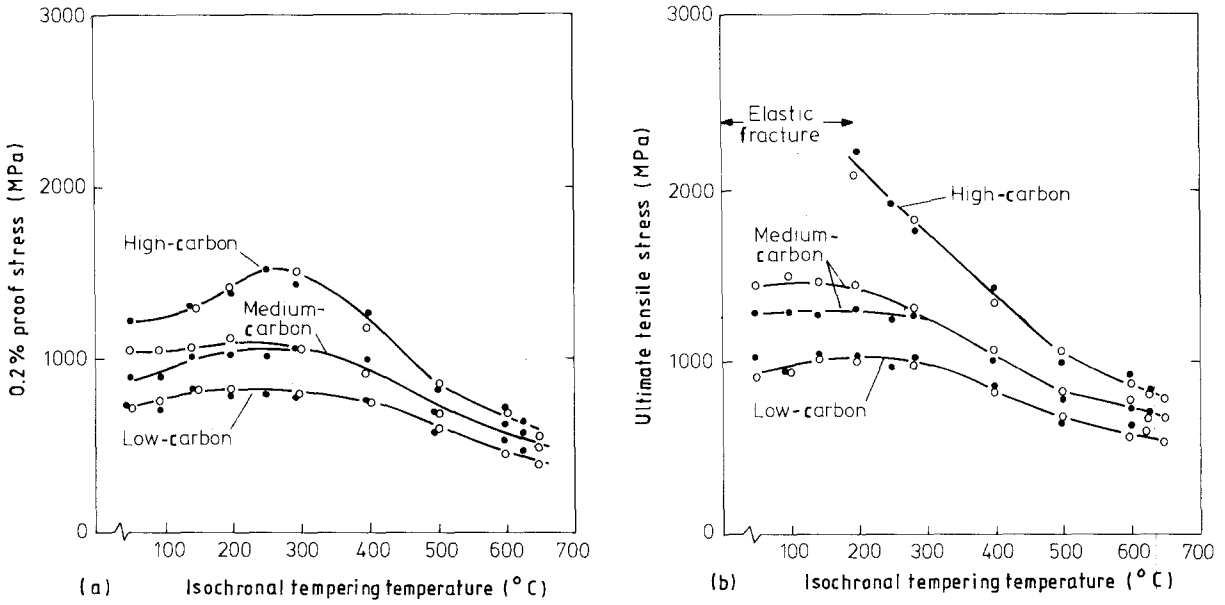

Figure 8 Effect of isochronal tempering upon (a) 0.2% proof and (b) ultimate tensile stresses of the six steels. (○) High-sulphide, (●) low-sulphide content. Steels: A, 0.054% C, 0.069% S; B, 0.197% C, 0.070% S; C, 0.494% C, 0.069% S; D, 0.060% C, 0.006% S; E, 0.169% C, 0.006% S; F, 0.486% C, 0.006% S.

The transition from alternating shear to cup and cone fracture is not an abrupt one. The most extreme cases of alternating shear generally occur in materials in an untempered state. No optically resolvable carbides are present, and the fracture surface contains no voids other than those associated with inclusions (Fig. 14). However, after tempering just below the transition tempering temperature, the inter-inclusion region is covered with a secondary distribution of fine voids, nucleated on carbides (Fig. 13). The transition in fracture mode is linked to the appearance of large carbides in the inter-inclusion ligaments, but may also depend upon other factors such as the remaining work-hardening capacity of the matrix and the magnitude of the local stress supported by the ligaments.

3.4.3. Brittle fracture

As-quenched and lightly tempered (< 300 °C) samples of high-carbon steel underwent a brittle mode of

TABLE IV Mechanical properties for Steels A, B and C as a function of isochronal tempering temperature

Steel	Tempering temperature (°C)	$\sigma_{0.1}$(MPa)	$\sigma_{0.2}$(MPa)	σ_{UTS}(MPa)	Strain to σ_{UTS}	Ductility(mm)	n
A	49	625	738	908	0.024	1.92	0.10
	97	648	773	955	0.017	1.74	0.07
	145	817	815	1013	0.026	1.48	0.08
	197	767	840	1003	0.025	1.25	0.07
	287	747	815	983	0.032	1.66	0.06
	403	764	783	937	0.030	2.14	0.03
	502	594	609	678	0.067	4.42	0.03
	601	450	472	569	0.104	6.64	0.02
B	49	931	1055	1469	0.039	1.51	0.12
	97	890	1053	1469	0.040	1.34	0.11
	145	954	1070	1459	0.044	1.56	0.11
	197	1030	1117	1446	0.030	1.53	0.09
	287	1014	1077	1304	0.034	1.49	0.06
	403	902	927	1060	0.038	1.60	0.05
	502	697	706	815	0.070	3.81	0.03
	601	461	467	567	0.108	5.52	0.02
C	49						0.01
	97						
	145	977	1310	1927	0.022	0.38	0.02
	197	1245	1412	2093	0.049	1.14	0.17
	287	1443	1513	1825	0.033	0.96	0.09
	403	1135	1191	1351	0.032	1.52	0.05
	502	817	762	1059	0.054	3.09	0.05
	601	704	713	875	0.093	4.48	0.03

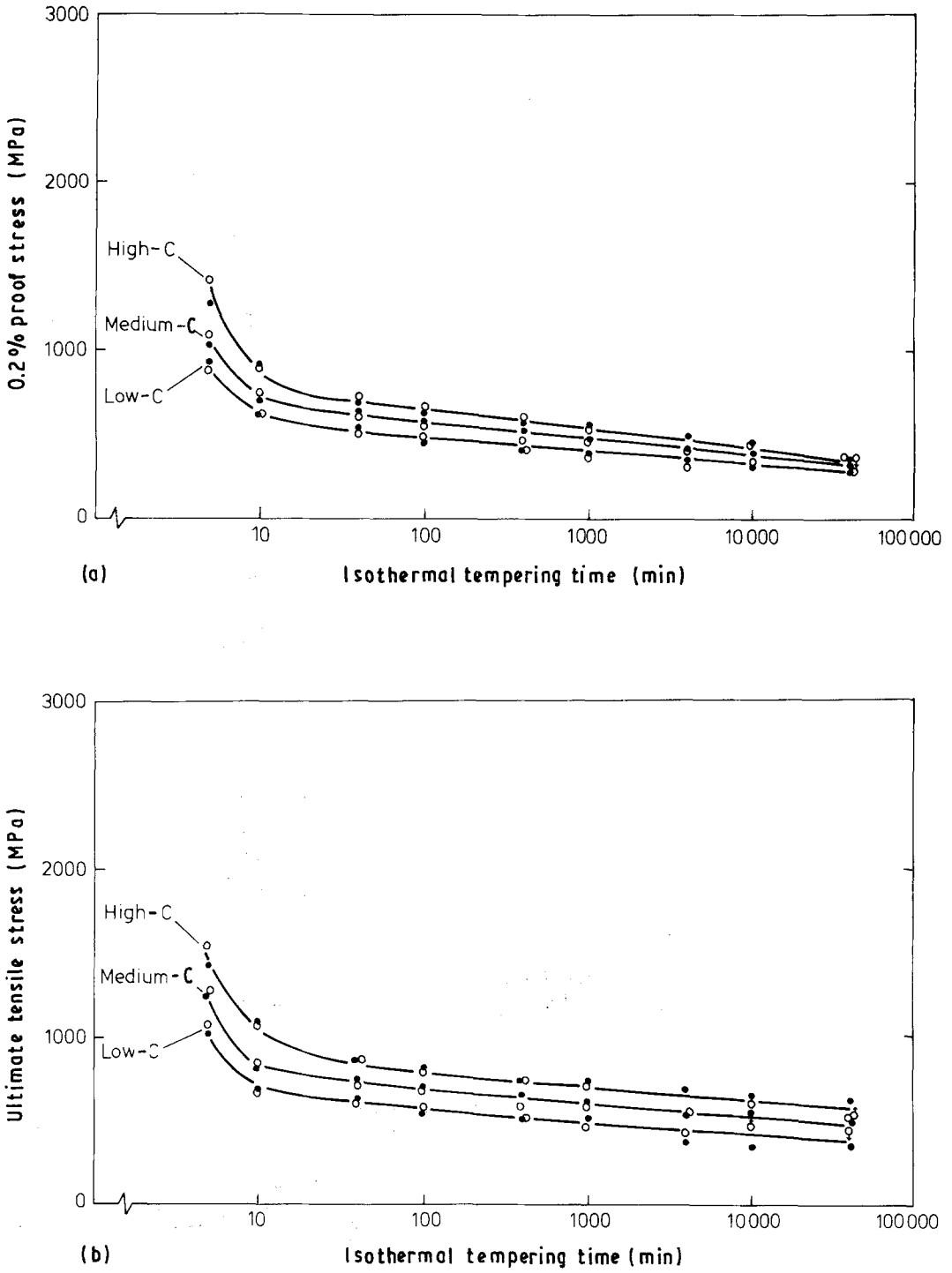

Figure 9 Effect of isothermal tempering at 625 °C upon (a) 0.2% proof and (b) ultimate tensile stresses of the six steels. (○) High-sulphide, (●) low-sulphide content.

fracture (Fig. 10c). The fracture initially nucleated at prior austenite grain boundaries (Fig. 15a), at the edge of the sample. This region of microcracking spread to form a semi-elliptical region covering about 10% of the cross-section. The fracture mode then changed to transgranular cleavage as the sample underwent final catastrophic failure (Fig. 15b).

We presume that the subcritical intergranular microcracking occurred during nominally elastic loading, and is the origin of the acoustic emission during elastic loading of rapidly cooled samples (Fig. 4e). The mechanism responsible for this fracture mode and the origin of the transition to cleavage has not been determined. However, the possibility of cracking occurring during quenching from 1000 °C has been eliminated. For instance, SEM studies of samples subjected to the same cooling rates following austenization showed no evidence of such cracking when tempered above 300 °C before testing. This tempering treatment would not "heal" cracks formed during the quenching process, and these defects would have nucleated ductile fracture and remained on the fracture surface.

4. Discussion

Experiments have been performed to observe the effects of an enhanced population of manganese

TABLE V Mechanical properties for Steels A, B and C as a function of isothermal tempering temperature

Steel	Temper time (min)	$\sigma_{0.1}$(MPa)	$\sigma_{0.2}$(MPa)	σ_{UTS}(MPa)	Strain to σ_{UTS}	Ductility(mm)	n
A	5	880	892	1075	0.020	1.62	0.09
	10	618	625	680	0.074	4.17	0.02
	40	522	522	615	0.115	6.95	0.01
	100	490	492	590	0.100	3.40	0.01
	400	428	425	526	0.184	3.74	0.01
	1000	372	375	484	0.156	3.00	0.01
	4000	315	320	449	0.175	3.97	0.01
	10000	351	351	483	0.189	4.93	0.01
	40000	316	316	462	0.210	4.96	0.01
B	5	1052	1099	1265	0.027	1.09	0.07
	10	745	759	759	0.061	3.1	0.03
	40	606	601	721	0.095	5.34	0.01
	100	567	567	684	0.097	2.40	0.01
	400	480	460	465	0.135	3.62	0.01
	1000	482	482	484	0.126	3.15	0.01
	4000	435	433	576	0.157	3.85	0.01
	40000	378	381	530	0.184	4.75	0.01
C	5	1390	1427	1555	0.017	0.68	0.05
	10	911	920	1050	0.062	1.36	0.04
	40	724	730	870	0.092	2.28	0.02
	100	663	670	809	0.091	2.32	0.02
	400	603	606	755	0.112	2.71	0.01
	1000	558	551	718	0.133	3.24	0.02
	10000	445	448	614	0.141	3.94	0.01
	40000	369	371	528	0.171	4.61	0.01

sulphide inclusions upon acoustic emission, mechanical properties and fracture behaviour of a model low-alloy steel system. When present in an approximately spheroidal form, a ten-fold inclusion increase causes a small, but measurable enhancement of the acoustic activity. The yield stress, ultimate tensile strength, and work-hardening exponent are essentially unaffected by the higher spheroidal inclusion concentration. This contrasts sharply with the situation beyond σ_{UTS} where the addition of spheroidal inclusions severely

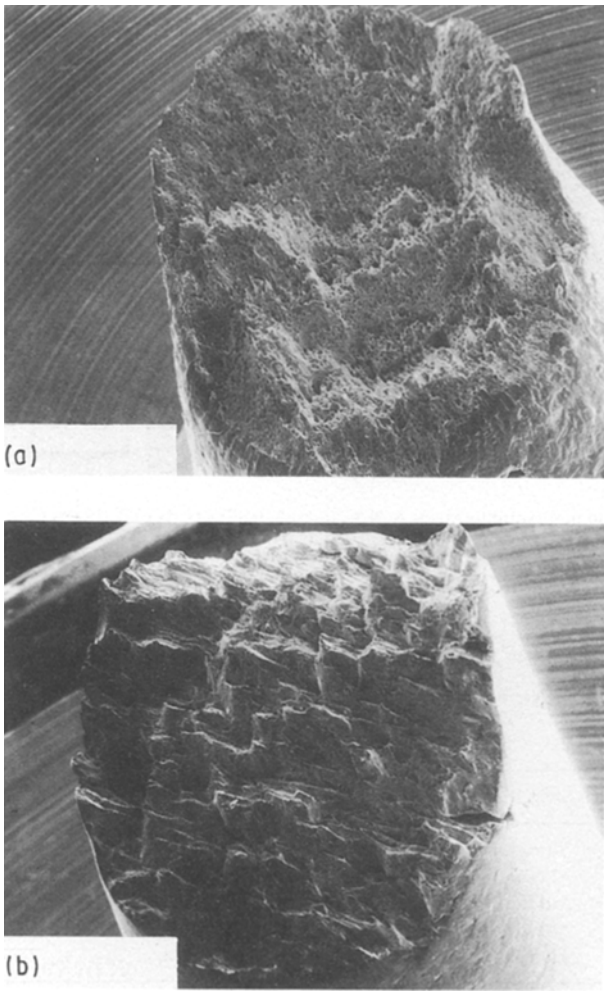

Figure 10 Effect of carbon content upon fracture morphology of high-sulphur Steels A, B, C, tempered for 100 min at 50 °C. (a) A, 0.054 wt% C, cup and cone; (b) B, 0.197 wt% C, alternating shear; (c) C, 0.494 wt% C, intergranular/cleavage.

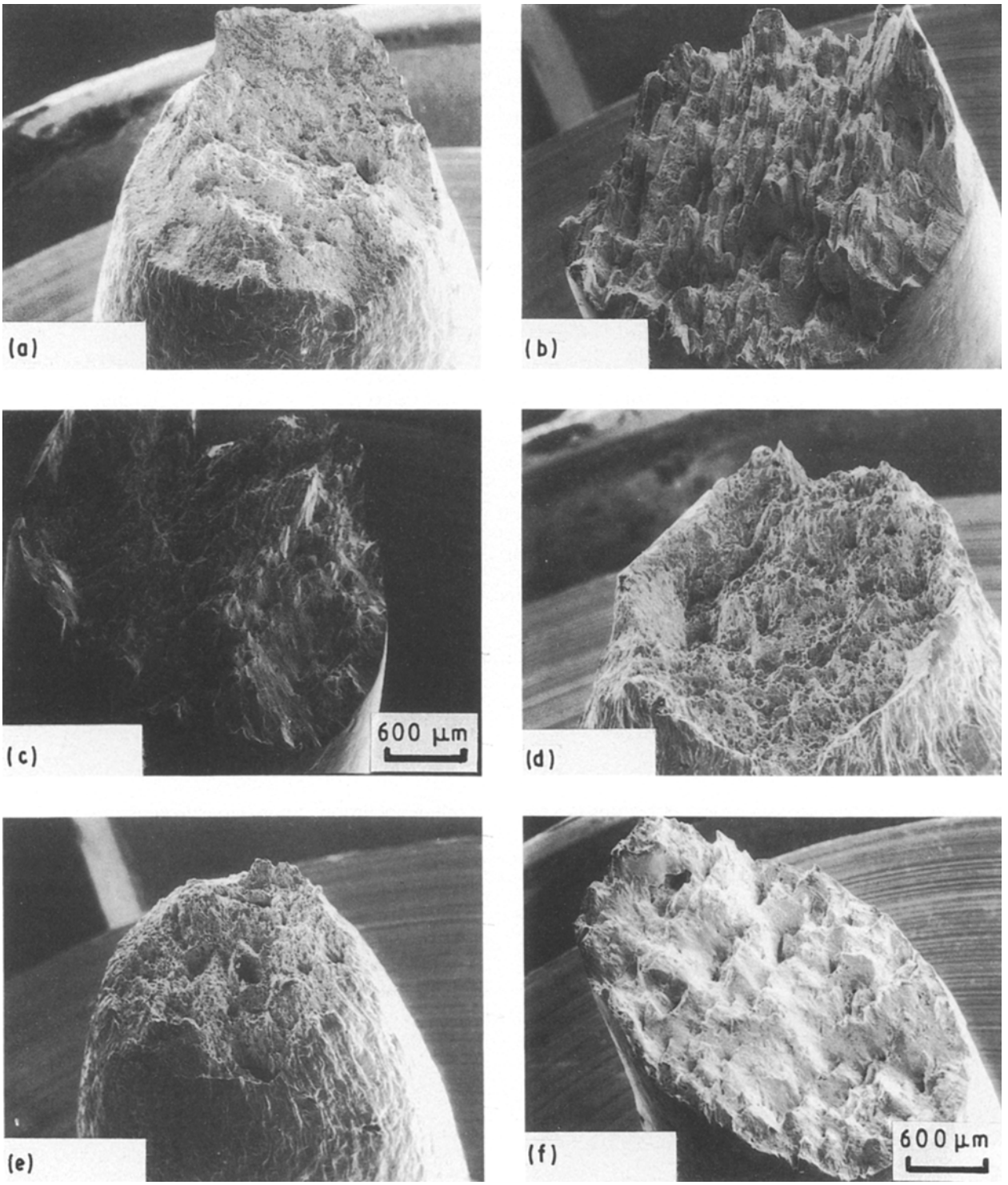

Figure 11 Effect of isochronal tempering at (a–c) 290 and (d–f) 600 °C upon high-sulphur Steels A, B, C. (a, d) A, 0.07% C; (b, e) B, 0.21% C; (c, f) C, 0.48% C.

TABLE VI Summary of microscopic fracture modes for high-sulphur steels

Heat treatment	Steel A	Steel B	Steel C
Oil quench	Cup and cone	Alternating shear	Intergranular cleavage
+ 300 °C, 100 min	Cup and cone	Alternating shear	Alternating shear
+ 625 °C, 10 min	Cup and cone	Alternating shear	Alternating shear
+ 600 °C, 100 min	Cup and cone	Alternating shear	Cup and cone
+ 625 °C, 1000 min	Cup and cone	Alternating shear	Cup and cone

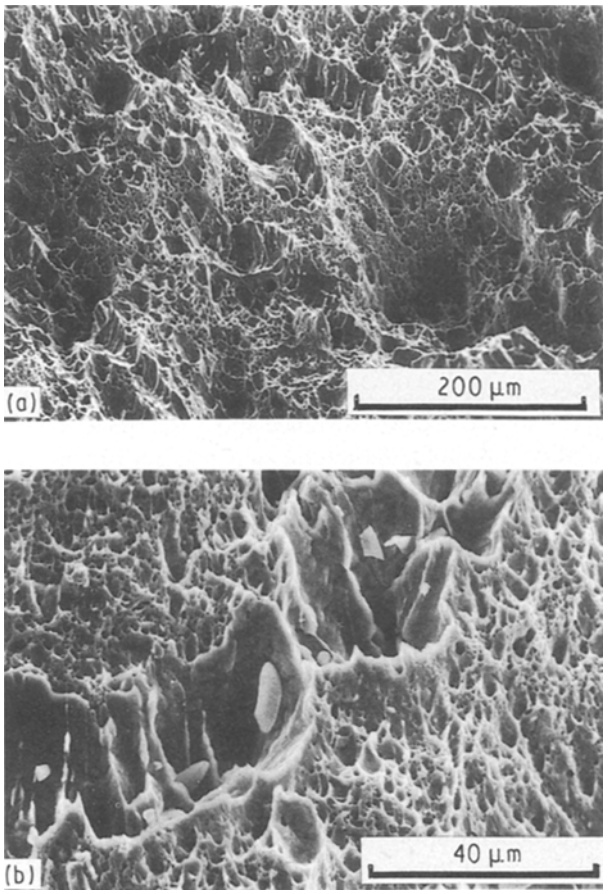

Figure 12 Central area of isochronally tempered Steel A that underwent ductile cup and cone fracture. (a) 403 °C, (b) 601 °C.

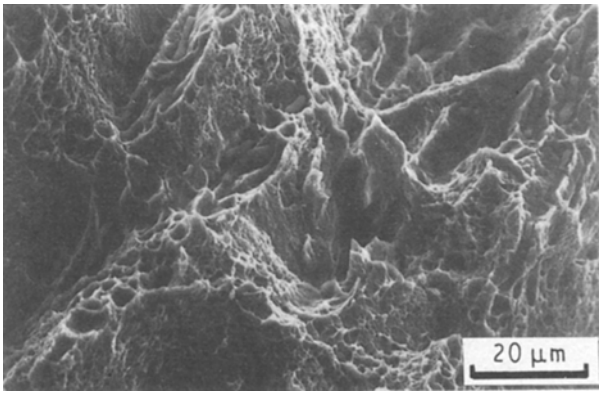

Figure 13 Fracture morphology of high-sulphur Steel C tempered for 100 min at 290 °C.

reduces non-uniform extension and extends the range of microstructures which exhibit alternating shear fracture, and with it, detectable acoustic emission during crack growth. The transition from alternating shear to brittle behaviour, however, seems less affected by the inclusion concentration.

4.1. Pre-σ_{UTS} deformation

We find that a factor of ten increase in sulphur concentration (and thus inclusion concentration) leads to an increase in acoustic emission energy per test of between 10% and 50%. This additional component of

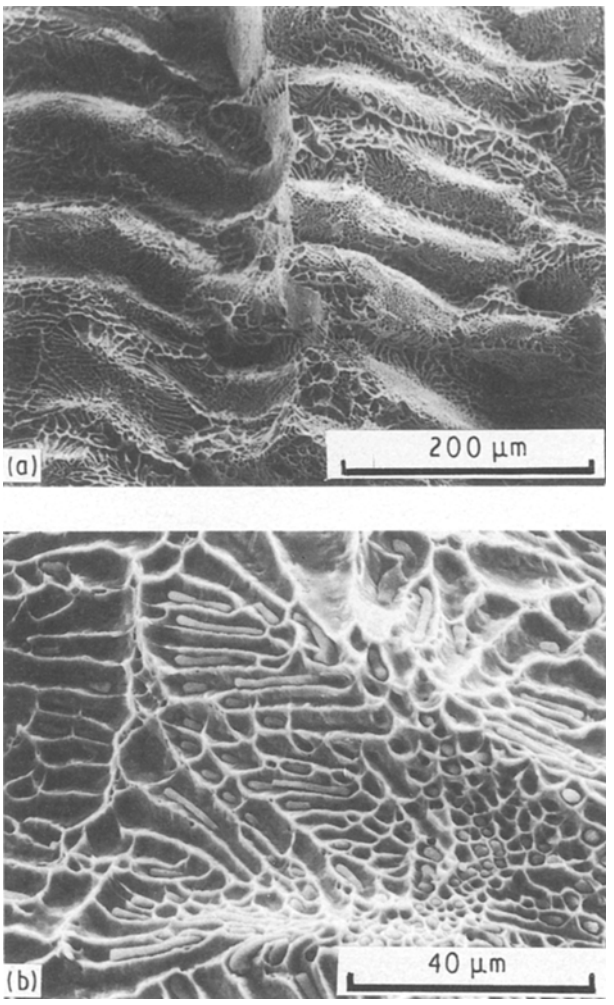

Figure 14 Alternating shear fracture typical of Steel B (oil quenched) showing influence of sulphide inclusion distribution.

emission occurs in the same strain range where the matrix emits acoustic emission (yield). The inclusion contribution shows two trends of interest. First, the contribution increases as the carbon content is raised. Secondly, when the extended region of brittle behaviour of Steel C is accounted for, the "inclusion component" is greatest for 300 °C tempers. The non-inclusion component of the low sulphur steels has been proposed to be individual "microyield" events for which the *nav* product (*n* is the number of dislocations, *a* the slip distance and *v* the dislocation velocity) exceeded a critical value, of the order of 0.03 $m^2 s^{-1}$ [2].

Two processes have been suggested to account for inclusion-related emission in steels. One process, first suggested by Ono *et al.* [8], considers the decohesion of the weak inclusion–matrix interface to be the source of emission. The second, proposed by Holt and Goddard [9], considers the stress concentration in the matrix near to an inclusion as a trigger for localized plastic deformation which generates detectable emission. In reality, both an abrupt drop in the local stress (the inclusion stress drops to zero) and a simultaneous plastic deformation of the adjacent matrix (due to the increased concentration of stress near the equator of the newly created void) occurs during decohesion. For example, the stress intensity in the matrix at the equator of a spherical hole is three times that of the

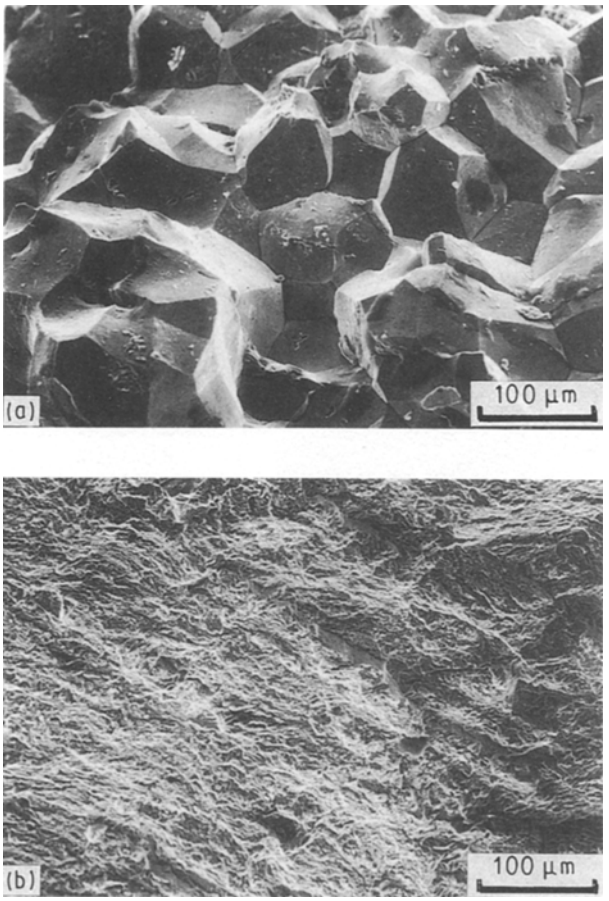

Figure 15 Typical examples of (a) intergranular and (b) cleavage fracture of quenched high-carbon Steel C.

remote stress. If the remote stress at which decohesion occurs then exceeds one-third of the matrix yield stress, the matrix at the equator would indeed yield. Both processes (the abrupt drop in stress and the ensuing matrix plasticity) could generate acoustic emission, but the latter would only be detectable if the mechanism of matrix plasticity were able to generate detectable emission (as occurs, for instance, in material tempered near 250–300 °C), and it would only result in an additional "inclusion" component to the total emission if the emission was amplified over and above that of the inclusion-free matrix.

Because matrix volume elements adjacent to inclusions would have generated signals in the absence of inclusions, the Holt and Goddard mechanism would not appear at first sight to lead to extra emission energy per test. To account for the observed increase in acoustic emission, the Holt and Goddard mechanism must enhance the emission signals from matrix volume elements adjacent to inclusions. As this is controlled by the product (nav) of the distance and velocity swept out by n dislocations, it implies that one or other or both are increased near the inclusion. Given the well-known strong dependence of dislocation velocity upon stress, it seems reasonable to expect that dislocation velocities in the stress concentration regions near inclusions will, on average, be larger and the nav value for individual events increased over those of low-inclusion content material. The resulting emission energy increase would be expected to depend upon heat treatment in a similar way to the matrix dependence, and this was indeed the trend observed.

It is also possible for the inclusion decohesion event itself to contribute to the detected acoustic emission [8]. If decohesion is assumed to occur at the inclusion poles, decohesion can be likened to horizontal Mode I microcracks opening in a homogeneous body (Fig. 16). To estimate if a decohesion event could then give rise to a detectable acoustic emission signal, we can use the acoustic emission detectability criterion for a microcrack given by Scruby *et al.* [3] $\sigma a^2 v > 5 \times 10^{14} hx$ (mks units, i.e. W), where σ is the remote stress, a the crack radius, v the radial crack speed, h the source–receiver distance and x the signal detectability threshold. Assuming that $h = 3 \times 10^{-2}$m and $x = 10^{-14}$m, $\sigma a^2 v > 0.15$ W for a detectable signal to be emitted [2]. Here, the value of σ corresponds to the average stress at the decohesion site just prior to fracture. Thus, it is a measure of the cohesive strength of the interface. Previous work on low-alloy steels indicates that this stress is in the range 300–600 MPa [10], but will also depend upon factors such as the degree of interfacial bonding (which is affected by segregation during heat treatment), the stress concentration at the interface (controlled by the inclusion shape and composition), and residual stresses that, in turn, depend upon the heat treatment.

Using the lower estimate of the decohesion stress (300 MPa), and assuming the interface undergoes a

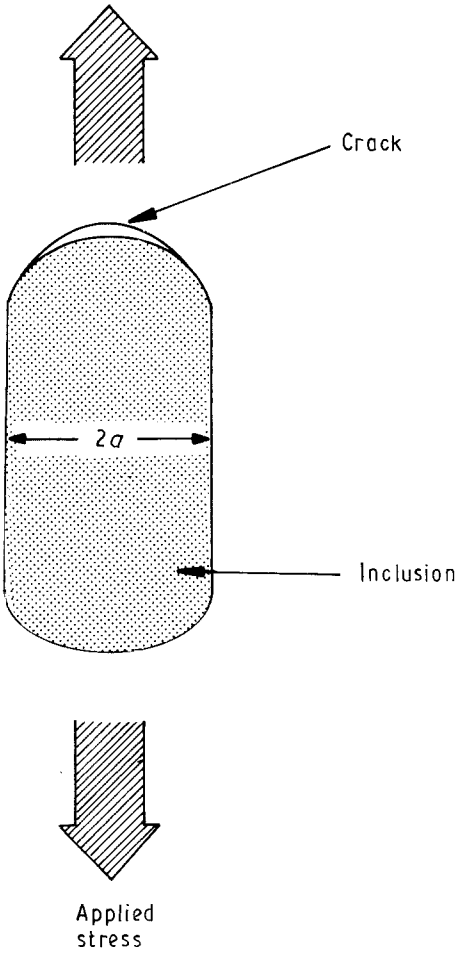

Figure 16 Interfacial decohesion at pole of manganese sulphide inclusion.

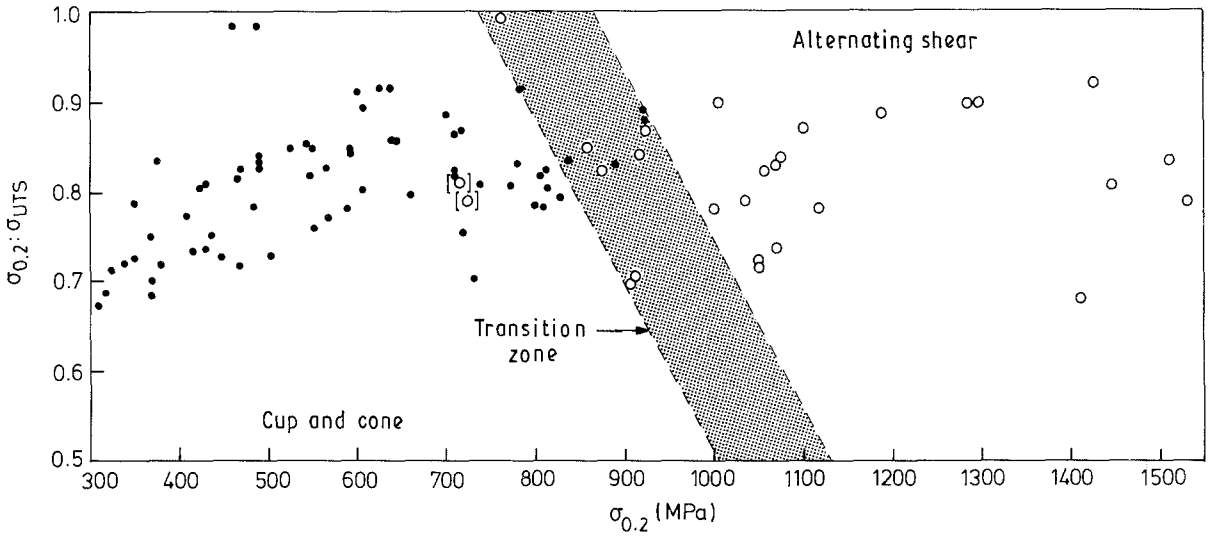

Figure 17 Effect of 0.2% proof stress and its ratio to ultimate tensile stress upon fracture mode for high- and low-sulphur steels. (●) Cup and cone, (○) alternating shear fracture.

brittle fracture for which v would be a significant fraction of the sound speed, say around 500 ms^{-1}, implies that all inclusions with diameter $> 2\,\mu m$ would contribute to detectable events. Higher cohesive strengths and cracking speeds increase both the fraction of the inclusion population that contribute to detectable signals and the acoustic emission energy from each event. Thus, the relative contribution of inclusion decohesion emission energy to a test will depend upon the inclusion size distribution and interfacial strength [11]. Fig. 2 also shows some evidence of inclusion fracture in addition to decohesion. The above calculations could be equally applied to such fracture events, and we conclude that they also could contribute some extra emission in high-inclusion content materials.

4.2. Post-σ_{UTS} deformation and fracture

Turning next to fracture, we note that a wide range of fracture modes, from intergranular through alternating shear to cup and cone, have been observed at ambient temperature. Inclusion content plays a role in each. Intense acoustic emission was observed during intergranular fracture, somewhat less emission during alternating shear and no emission from cup and cone fracture.

Suppose we consider a typical element of intergranular fracture to be the brittle separation of a single grain facet. Using typical values for a $\sim 10\,\mu m$, $v \sim 1000$ m s^{-1} and $\sigma \sim 1000$ MPa, we find $\sigma a^2 v \simeq$ 100 W, which would give rise to a very energetic acoustic emission. Thus, each emission from the samples (e.g. Fig. 4) undergoing intergranular fracture could be due to the creation of intergranular microcracks (and their coalescence to form a critical defect). The number of emissions observed during the test is comparable with the number of intergranular facets observed, suggesting that the fracture of these was responsible for each discrete signal.

A dominant event during the alternating shear fracture mode is the unstable shear of an inter-inclusion ligament. A typical inter-inclusion separation distance is 10 μm and the local stress at which the instability initiates is ~ 1000 MPa. Assuming a velocity of 500 m s^{-1}, $\sigma a^2 v = 50$ W; again an intense acoustic source, easily capable of causing the observed strong signals. Again the number of signals and shear facets are similar, suggesting that each discrete event is associated with the formation of a single facet.

We note this mode of fracture is only associated with a limited range of microstructures. The propensity for shear fracture is thought usually to correlate with a decrease in work-hardening capacity of the matrix. Plotting the fracture mode on a map of $\sigma_{0.2}$: σ_{UTS} (a crude work-hardening capacity parameter) against $\sigma_{0.2}$ (Fig. 17), we see that the alternating shear process is, in fact, favoured by a high yield strength. We see that the dependence on work-hardening capacity is much weaker. High yield strengths are obtained from microstructures with a dense distribution of very small carbides. Microvoid nucleation and coalescence at the carbides leads locally to a soft zone and intense plastic instability [12, 13]. The propensity for shear fracture in higher yield-strength materials presumably reflects the more rapid attainment of a void nucleation stress and a greater driving force for unstable fracture.

This mechanism of unstable shear fracture depends both upon the inter-inclusion spacing (which determines the load supported by the ligament and thus the stress at the carbide interface), and the size and spacing of the carbides. Experimentally, we have observed that as the carbide size and spacing increases. (i.e. the yield strength decreases) the cup and cone fracture is promoted. Increasing the inclusion spacing reduces the range of carbide sizes and spacings that lead to a shear fracture.

This emerging understanding of shear-facet formation leads naturally to a cup and cone fracture as the carbide size and spacing increase. Then only a few carbides are present between the inclusions, the area of material supporting the load is large, the work-hardening capacity high, and plastic hole growth becomes the favoured mode of deformation. Final ligament failure occurs by the overlap of holes nucleated at carbides [13] and accounts for the observation of a

correlation between inter-inclusion void density on fracture surfaces and the carbide density. It also accounts for the decrease in plastic extension after σ_{UTS} in high-sulphur material because of the reduced area that supports the applied load. The process of stable hole growth and coalescence can alternatively be viewed as the formation of a microcrack at close to zero velocity, radiating therefore almost zero elastic wave energy in the frequency regime used for acoustic emission detection.

5. Conclusion

The acoustic emission of quenched and tempered steels, and their post σ_{UTS} strains are found to be significantly affected by inclusion content, in particular:

1. Raising the sulphur content of low-alloy steels leads to enhanced concentrations of approximately spheroidal inclusions which are observed to increase acoustic emission during plastic deformation by 10%–50%. The most likely mechanisms for this additional emission are microplastic events in the matrix adjacent to inclusions together with inclusion decohesion from the matrix.

2. Inclusion content has little effect on the emission from brittle fracture. In contrast, increasing the sulphide concentration, and hence decreasing the inclusion spacing, tended to promote ductile cup and cone rather than alternating shear fracture in tempered material. There was an attendant reduction in emission from the alternating shear fracture.

3. Inclusion content strongly affects non-uniform strain in these steels. Increasing the inclusion content reduces the post-σ_{UTS} strain to fracture. The effect is also influenced by tempering, samples tempered at 300 °C showing a minimum in post-σ_{UTS} strain to fracture. Increasing the carbon content also reduces this parameter.

Acknowledgements

We wish to thank Drs B. L. Frye, B. Pickering, J. Hudson and C. A. Hippsley for stimulating discussions of this work, and P. Lane and A. Bartlett for their practical assistance with the research. This work was funded by United Kingdom Ministry of Defence (Procurement Executive) through ARE (Holton Heath).

References

1. H. N. G. WADLEY, C. B. SCRUBY and J. H. SPEAKE, *Int. Met. Rev.* **3** (1980) 41.
2. C. B. SCRUBY, H. N. G. WADLEY and J. E. SINCLAIR, *Phil. Mag.* **44** (1981) 249.
3. C. B. SCRUBY, C. JONES, J. M. TITCHMARSH and H. N. G. WADLEY, *Metal Sci.* **15** (1981) 241.
4. H. N. G. WADLEY and C. B. SCRUBY, *J. Mater. Sci.* **26** (1991) 5777.
5. C. B. SCRUBY and H. N. G. WADLEY, *ibid.*, **28** (1993) 2501.
6. G. T. HAHN, M. F. KANNINEN and A. R. ROSENFIELD, *Ann. Rev. Mater. Sci.* **2** (1972) 381.
7. A. S. ARGON, J. IM and R. SAFOGLU, *Metal Trans.* **6A** (1975) 825.
8. K. ONO, G. HUANG and H. HATANO, in "Proceedings of the 8th World Conference on NDT", Cannes, France (1976).
9. J. HOLT and D. J. GODDARD, *Mater. Sci. Engng* **44** (1980) 251.
10. H. N. G. WADLEY, D. C. FURZE, C. B. SCRUBY and B. L. EYRE, *Met. Sci.* (1979) 451.
11. L. M. BROWN and J. D. EMBURY, in "Third International Conference on Strength of Metals and Alloys" (Institute of Metals, London, 1973) p. 164.
12. H. COUQUE, R. J. ASARO, J. DUFFY and S. H. LEE, *Met. Trans.* **19A** (1988) 2179.
13. S. H. GOODS and L. M. BROWN, *Acta Metall.* **27** (1979) 1.

Received 21 July
and accepted 2 September 1992